Evaluation of Structural and Optical Properties of Mn-Doped ZnO Thin Films Synthesized by Sol-Gel Technique

EYÜP F. KESKENLER, SEYDI DOĞAN, GÜVEN TURGUT, and BEKIR GÜRBULAK

Undoped ZnO and Mn-doped ZnO (MZO) films with 0.25, 0.50, and 0.75 mol pct were synthesized onto glass substrates by sol-gel spin-coating technique, and the effects of Mn on structural, morphologic, and optical properties were investigated. The XRD results indicate that the films have wurtzite structure with polycrystalline nature. However, the dominant peak was (002) diffraction peak for all samples; other diffraction peaks with less intensity such as (100), (101), (102), (110), (103), (112), and (004) were observed for the undoped ZnO. The lattice parameter values of MZO thin films were lower than that of the undoped ZnO. Plane stress values indicated that the films had the tensile stress. A decrease in the grain sizes was observed with the increasing Mn mole percent. The optical transmission values were found to be 82 pct for the undoped ZnO and 80, 78, and 75 pct for the MZO with 0.25, 0.50, and 0.75 mol pct, respectively, at the wavelength of 405 nm. The optical band gap values decreased from 3.287 to 3.270 eV, the surface roughness values increased from 58.13 to 60.67 nm, Urbach energy values increased—a 18.3-meV difference in Urbach energy was observed—and in addition, the steepness parameters decreased with increasing Mn content from 0 to 0.75 mol pct.

I. INTRODUCTION

SEMICONDUCTOR nanocrystalline structures have attracted great interest in view of their photonic and electronic device applications.[1] In recent years, widespread utilization of these metal oxides has led to the increased interest in respect of various applications of these semiconductor thin films. In oxides, Zinc Oxide (ZnO) is an attractive candidate for optoelectronic applications, and being a member of II-VI semiconductor family with a large excitation binding energy (60 meV) and a wide band gap (3.37 eV).[2] ZnO, it also enjoys a unique position among materials owing to its superior and diverse properties such as piezoelectricity, chemical stability, biocompatibility, optical transparency in the visible region, high voltage-current nonlinearity, large bond strength, *etc*.[3] These characteristics of ZnO have shown important properties for some special applications such as solar cells,[4–8] surface acoustic wave guides,[9] sensors,[10–12] transparent electrodes,[13] UV laser,[14] ultraviolet light emitting, and laser diodes.[15]

On the other hand, dilute magnetic semiconductors (DMSs) have attracted significant attention for the past several decades because of their combination of usual semiconductor features and a polarized electron spin state associated with a replaced transition-metal ion.[16] Currently, much experimental study and theoretical research have especially focused on studying the properties of DMSs based on ZnO doped with transition metal ions such as Co and Mn. Magnetic ions (Mn^{2+}, Co^{2+}, V^{2+}, Fe^{2+}, Cr^{2+}, *etc*.) should occupy interstitial sites or substitute some of the metallic atoms in the semiconductor lattice to produce a magnetic semiconductor. The mechanism leading to room temperature ferromagnetism in Mn-doped ZnO (MZO) is not fully established, and there are many contradictory experimental observations.[17] However, it is stated that oxygen has a tendency to pull electrons away from other atoms in the compounds resulting in a strong electrical field occurring at the interatomic scale. These fields can give rise to substantial correlations, which exhibit dominant ferromagnetic behavior between the electrons of one atom and those of its neighbors.[18] Thus, many experimental groups have attempted to grow ZnO semiconductors doped with ferromagnetic transition metals (Mn, Co, V, Fe, Cr, and Ni)[16] to understand the mechanism of ferromagnetism fully.

The MZO (ZnO:Mn) thin films have been the subject of a number of recent studies, and different growth techniques, such as chemical vapor deposition (CVD),[19,20] radio frequency magnetron sputtering (RFMS),[21] molecular beam epitaxy,[22,23] pulsed laser deposition (PLD),[24–26] and sol-gel technique,[27–31] have been used to grow the films. The results in respect of ferromagnetism in different doping concentrations are still controversial, and it has been reported that the magnetic properties in oxides films are very sensitive to the preparation method.[32,33]

EYÜP F. KESKENLER, Research Assistant Dr., is with the Department of Physics, Faculty of Arts and Sciences, Recep Tayyip Erdoğan University, 53100 Rize, Turkey, Contact e-mail: eyupfahri.keskenler@rize.edu.tr SEYDI DOĞAN, Professor Dr., and BEKIR GÜRBULAK, Assistant Professor Dr., are with the Department of Physics, Faculty of Science, Atatürk University, 25240 Erzurum, Turkey. GÜVEN TURGUT, Research Assistant, is with the Department of Physics, Kazım K. Education Faculty, Atatürk University, 25240 Erzurum, Turkey.

In the current study, it is aimed to comprehensively explore the structural and optical properties of the undoped ZnO and ZnO:Mn (0.25, 0.50, and 0.75 mol pct Mn-doped) thin films grown on lamella glass substrates by simple and low cost sol-gel spin-coating technique. The doping concentration was chosen less than the equilibrium solubility limit of Mn^{2+} ions in ZnO. Sol-gel spin-coating technique was preferred for the synthesis of ZnO:Mn thin films, because of the many advantages of this process, such as better stoichiometry control, better homogeneity, lower cost, possibility of using high-purity starting materials, low processing temperature, and having an easy coating process of large substrates. Earlier, we have published an article about the successful growth of the undoped nanocrystalline ZnO thin films using this technique.[34]

II. EXPERIMENTAL DETAILS

A. Synthesis

The undoped ZnO and ZnO:Mn thin films were grown on glass substrates by spin coating sol-gel technique. The basic precursor solution was prepared by means of Zinc acetate dihydrate [$Zn(CH_3COO)_2 \cdot 2(H_2O)$] as a starting material. 2-Methoxyethanol ($C_3H_8O_2$) and monoethanolamine (C_2H_7NO, MEA) were used as solvent and stabilizer, respectively. For the MZO (ZnO:Mn) solution, the manganese (III) acetate dihydrate [($C_6H_9MnO \cdot 2(H_2O)$] was dissolved in the solution for being used as the manganese source. The molar ratios of metals to MEA were fixed in the ratio of 1:1. Zinc acetate dihydrate (0.5 M) and manganese acetate dihydrate (0.5 M) were mixed in different solution mole ratios from 0.25 to 0.75 mol pct with 0.25 as incremental step. The undoped ZnO was used as a reference sample. The prepared solution was stirred at 343 K (70 °C) for 4 hours to obtain a clear and homogenous solution in balloon flask which is tightly sealed. The glass substrates were cleaned using soap solution, de-ionized (DI) water, acetone, and methanol by means of an ultrasonic cleaner. Then, the substrates were rinsed with DI water and dried with nitrogen. The prepared precursor solution were spin coated on glass substrates placed on the sample holder kept rotating at a speed of 3000 rpm for 30 seconds by means of a spin-coater. The as-coated film was sintered at 473 K (200 °C) for 10 minutes to evaporate the solvent and remove the organic sediments to help achieve the good crystallinity, and then cooled down to room temperature. This process was repeated 10 times to obtain the intended thickness (about 0.5 μm) and the film with good quality. The same process was repeated for the films prepared under different values of manganese doping, and finally, they were annealed in air at 773 K (500 °C) for 30 minutes.

B. Characterizations

The structure and lattice parameters of the undoped ZnO and MZO films were analyzed at room temperature using a X-ray diffractometer (XRD) with $\lambda = 1.5418$ Å. The values of 2θ were altered between 25 deg and 80 deg. Morphologic properties of the films were observed by dynamic mode atomic force microscopy (D-AFM) (produced by Nanomagnetics-Inst). AFM images were obtained at 5×5 μm planar in tapping mode, in 512×512 resolutions, and with the speed of 3 μm/s. The optical transmittance of the thin films were recorded in the spectral region of 300-650 nm at room temperature using a Perkin Elmer UV/VIS Lambda 2S Spectrometer which works in the range of 190-1100 nm and has a wavelength accuracy of better than ±0.3 nm.

III. RESULTS AND DISCUSSION

A. XRD Analysis

Figure 1 shows the XRD pattern of the undoped ZnO and MZO thin films with the different mole percent values of Mn concentration on glass substrates. The XRD patterns of these samples are almost close to the values of the JCPDS Standard (No. 36-1451) data of wurtzite (or hexagonal) ZnO. These spectra clearly indicate that the films have polycrystalline nature with the preferred orientation being perpendicular to the substrates, same as results of Ruan et al.[15] Any of secondary phases related to oxides or groups of Mn were not observed. Maiti et al.[35] have also observed the similar results. Mn forms stable phases over a wide range when it substitutes in an II-VI group compound, and it is different from the other transition metals with the same property. Mn substitutes for the group II
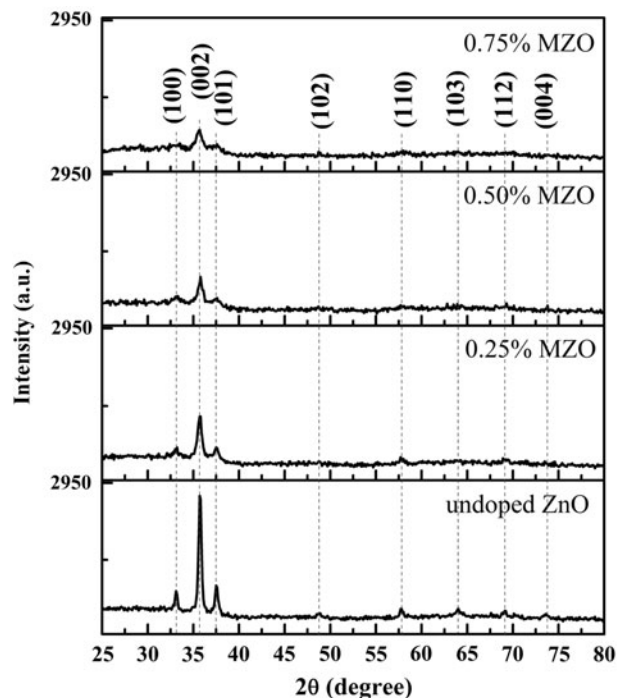

Fig. 1—XRD spectra of undoped ZnO and MZO thin films doped with the different mole percent values of Mn.

elements in the zinc-blende and wurtzite structures because the 3d orbitals of Mn are half-filled, and this affords great ease in the process.[36] Transition metals such as Mn having partially filled d orbitals have been effectively used as magnetic atoms in ZnO DMSs.[37]

As clearly seen from Figure 1, the XRD peak intensities decrease with an increase in the Mn doping ratio. Consequently, the crystal quality of the films undergoes deterioration, and this is directly related to the formation of an amorphous phase. It is found that dominant diffraction peak for the undoped ZnO and MZO thin films was the (002) line. For the undoped samples, in addition to this (002) peak, some additional peaks, which are comparatively lesser in intensity and corresponding to (100), (101), (102), (110), (103), (112), and (004) orientations, were also observed. When Mn was incorporated to ZnO structure, the other peaks began to disappear with the increasing Mn concentration except (100), (101), and (102) peaks. The highest intensity of the XRD peaks was obtained from the undoped ZnO film which was exhibiting a better crystal quality. When Mn was incorporated into the film, the intensity of the peak corresponding to (002) the plane decreased with doping concentration, and the intensities of other peaks continuously decreased with increasing Mn content as well. This result clarifies that the Mn atoms in the MZO films have been segregated into grain boundaries, and this results in restricting the crystallization of preferred orientation of ZnO. Similar results are also found in Reference 36. It can be seen that, by comparing the standard and calculated d values, all peaks are found to match the wurtzite (or hexagonal) structure of ZnO film. The lattice parameters a and c of the wurtzite structure of ZnO film can be calculated using the following relation:

$$\frac{1}{d^2} = \frac{4}{3}\left(\frac{h^2 + k^2 + hk}{a^2}\right) + \left(\frac{l^2}{c^2}\right) \quad [1]$$

where d is the interplanar distance, and (hkl) are the miller indices. The standard and calculated d values for (002), (100), and (101) dominant peaks of the undoped ZnO and MZO thin films are given in Table I. The calculated a and c lattice parameters are given in Table II, and they are almost close to the values of the JPCDS card no: 36-1451. As seen from the Table II, Mn doping affects the lattice parameters of ZnO. The lattice parameters of MZO thin films are slightly lower than those of the undoped ZnO. The crystallite sizes (D) of the

undoped ZnO and MZO films were calculated using the following Scherrer's formula[38];

$$D = \frac{0.9\lambda}{\beta \cos\theta} \quad [2]$$

where λ is the wavelength of the X-ray (1.5418 Å), β is the broadening of diffraction line measured at the half of its maximum intensity in radians, and θ is the diffraction angle. The calculated grain size values are given in Table II, and from Table II, it is seen that the grain size continuously decreased with increasing Mn doping ratio. The full width at half maximum (FWHM) for (002) peak and D values along with the 2θ values for (002), (100), and (101) peaks are also given in Table II for the undoped ZnO and MZO thin films. There were slight shifts in (002), (100) and (101) peak positions, owing to Mn atoms which both have different ion sizes and are segregating at the grain boundaries in the MZO films.

Plane stress (σ) of hexagonal crystals was calculated according as the biaxial strain model given by[39]

$$\sigma = \left[\frac{2C_{13} - C_{33}(C_{11} + C_{12})}{C_{13}}\right]\left(\frac{c - c_0}{c_0}\right) \quad [3]$$

where c_0 is the corresponding bulk value (0.5207 nm), c is the lattice parameter obtained from the (002) diffraction in the XRD, and C_{ij} are the elastic stiffness constants ($C_{11} = 2.1 \times 10^{11}$ N/m^2, $C_{12} = 2.1 \times 10^{11}$ N/m^2, $C_{13} = 2.1 \times 10^{11}$ N/m^2, and $C_{33} = 2.1 \times 10^{11}$ N/m^2). The stress can be obtained by the following simplified relation:

$$\sigma = -2.2 \times 10^{11}\left(\frac{c - c_0}{c_0}\right)(\text{N/m}^2) \quad [4]$$

The calculated results are listed in Table III. The negative and positive signs indicate the compressive and tensile stresses on the films, respectively. The total stresses in the film collectively depend on two factors: intrinsic and extrinsic stresses which are induced by defects and impurities in the crystal by the lattice mismatch between the film and substrate, respectively.[15] As seen in Table III, the increase in the mole percent of Mn in the structure increases the strain in the films. It has been pointed out that the residual stress may change the lattice spacing and band gap.[40] The altered stress, depend on c axis, might change the

Table I. The Standard and Calculated d Values for (002), (100), and (101) Main Peaks of Undoped ZnO and MZO Thin Films

(hkl)	Standard d (nm)	Observed d (nm)			
		Undoped ZnO	0.25 pct MZO	0.50 pct MZO	0.75 pct MZO
(100)	0.2814	0.2788	0.2698	0.2689	0.2671
(002)	0.2603	0.2519	0.2510	0.2508	0.2505
(101)	0.2475	0.2399	0.2398	0.2390	0.2390

Table II. The Lattice Parameters, Interplanar Distance (D), FWHM for (002) Peak, and 2θ Values Obtained from XRD Curves for Undoped ZnO and MZO Thin Films

Mn (Mol Pct)	Lattice Constants (nm)		D (nm)	FWHM (deg)	2θ (deg)		
	a	c			(002)	(100)	(101)
0.00	0.3220	0.5038	25.60	0.3407	35.638	32.100	37.496
0.25	0.3115	0.5019	16.58	0.5264	35.777	33.210	37.498
0.50	0.3105	0.5015	16.11	0.5419	35.808	33.320	37.635
0.75	0.3084	0.5010	11.99	0.7277	35.846	33.550	37.636

JPDS card no: 36-1451; standard values of $a = 0.3250$ nm and $c = 0.5207$ nm.

Table III. Roughness, rms, Stress, Urbach Energy, Steepness Parameter and Band Gap Values for Undoped ZnO and MZO Thin Films

Mn (Mol Pct)	Roughness (nm)	rms (nm)	Stress (N/m^2)	Urbach Energy (E_U) (meV)	Band Gap (eV)	Steepness Parameter (δ)
0.00	58.13	60.23	7.12×10^9	14.5	3.287	178.1×10^{-2}
0.25	58.51	61.33	7.93×10^9	23.0	3.279	112.3×10^{-2}
0.50	59.32	61.69	8.10×10^9	29.3	3.273	88.1×10^{-2}
0.75	60.67	63.45	8.32×10^9	32.8	3.270	78.7×10^{-2}

wave-functions, increase or decrease the separation between the conduction and valence bands and therefore leading to a shift in band gap.[41] It is also suggested that the lower internal stresses causing good crystalline quality in the films lead to their higher carrier mobility.[42] The electrical conductivity of ZnO films follows a linear relationship with their d-spacing, stress and density. Chu et al.[43] reported that post deposition annealing in vacuum of ZnO thin films on a silicon substrate improved the film structure and electrical characteristics, resulting in a smooth surface, dense structure, stress relief and increasing resistivity. The disorder and stress of the film are reduced by annealing. It often decreases the d-spacing. On the other hand, high temperature oxidation of metallic Zn and O incorporation may increase the d-spacing. Therefore annealing, particularly in air, could result in over stoichiometric O content and an increase in d-spacing.

B. AFM Analysis

Atomic force microscope (AFM) was used to investigate the surface topography of the films over a 5×5 μm area by tapping mode. AFM (2D and 3D) studies of the surface morphologies for the undoped ZnO and MZO thin films shown in Figure 2. As seen from the AFM images, the grain growth is perpendicular to the substrate surface. The surface roughness and root mean square (rms) values of the films are given in Table III. The surface roughness increases with increasing Mn content from 0.25 to 0.75 mol pct with rms increasing from 61.31 to 63.45 nm.

C. UV-Vis Analysis

Figure 3 shows the room temperature optical transmittance in the UV-vis region ranging from 300 to 650 nm and 380 to 420 nm for the undoped ZnO and MZO thin films with different Mn content. The optical transmission values, at the wavelength of 405 nm, were found to be 82 pct for the undoped ZnO and 80, 78 and 75 pct for the MZO with 0.25, 0.50 and 0.75 mol pct, respectively. These results suggest that the films have high transparency and an increase in the Mn content slightly decreases the transmittance. The optical absorption theory gives the relationship between the absorption coefficients (α) and the photon energy (hv) for the direct transition. The optical band gap values can be calculated by the following relation[34]:

$$(\alpha h v) = B(h v - E_g)^m \qquad [5]$$

where α is the absorption coefficient, hv the photon energy, B a constant, and E_g is the optical band gap. Since ZnO film has a direct optical transition.[35,44] In k-space, the direct transitions occur across the band gap between the conduction and the valence band edges. The total momentum and energy of the electron-photon system must be conserved in this process.[45] The direct optical band gap is obtained using this equation when the straight line portion of the $(\alpha h v)^2$ vs. hv plot is extrapolated to intersect the energy axis at $\alpha = 0$. Plot of $(\alpha h v)^2$ against hv for the undoped ZnO and MZO films is given in Figure 4. The obtained optical band gap values of the films are given in Table III. The optical band gap values of the films were decreased a little with increasing content of Mn in ZnO. As a result, increasing content of Mn in ZnO structure causes band gap shrinkage. The results obtained by Sinha et al. showed that the change in structure of the composite from crystalline to amorphous had caused a shift of the absorption edges toward the higher wavelength region. This behavior has been attributed to both the defect states, and disorders (especially dopants) which are producing band tails and narrowing band gap.[46]

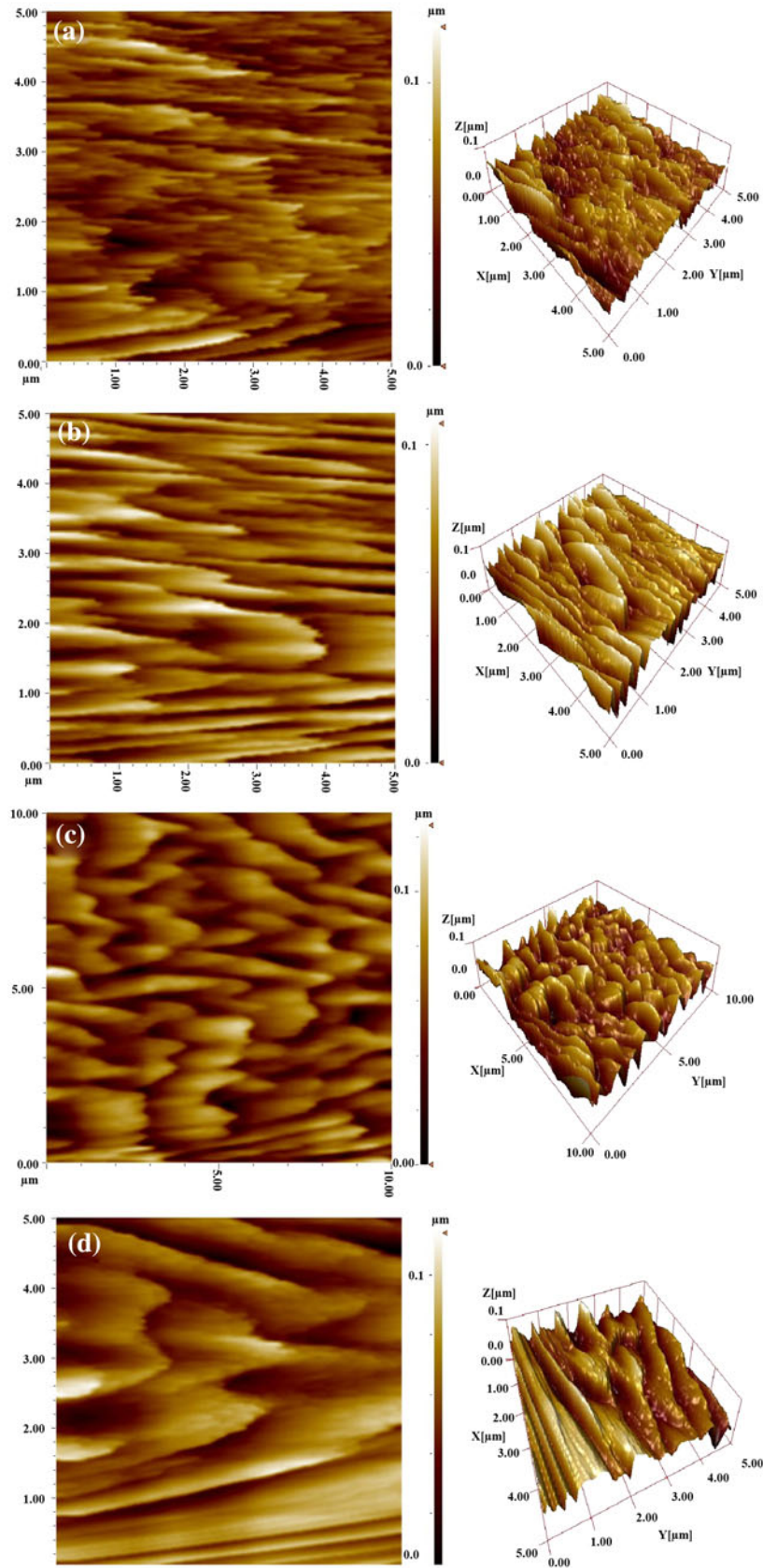Figure 5 shows the optical band gap values vs. different mole percent values of Mn content for the

Fig. 2—AFM images (2D and 3D) of undoped ZnO and MZO thin films (5 × 5 μm planar in tapping mode, in 512 × 512 resolutions and with speed of 3 μm/s) (a) undoped; (b) 0.25 mol; (c) 0.50 mol pct; (d) 0.75 mol pct.

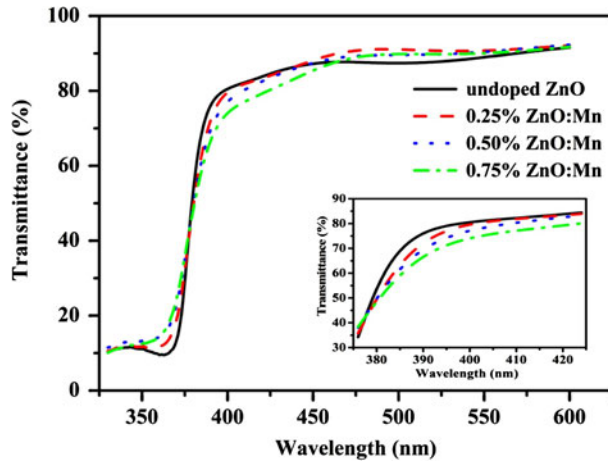Fig. 3—Optical transmittance spectra of undoped ZnO and MZO thin films.

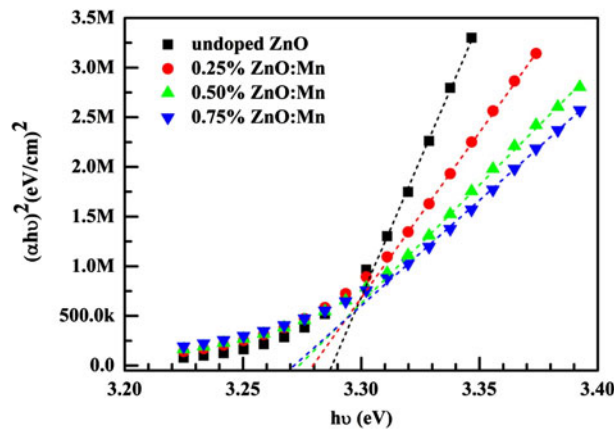Fig. 4—The plots of $(\alpha h\upsilon)^2$ vs. photon energy ($h\upsilon$) for the undoped ZnO and MZO thin films.
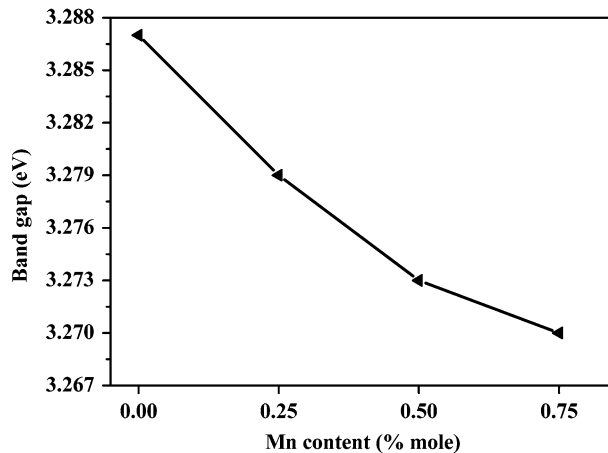

Fig. 5—Plot of band gap variations vs. different mole percent of Mn.

undoped ZnO and MZO (0.25, 0.50, and 0.75 mol pct Mn doped) thin films. As clearly seen from Figure 5, optical band gap values get reduced from 3.287 to 3.270 eV.

An exponentially increasing absorption edge in a number of insulators, including ionic crystals, semiconductors, and organic crystals follows the empirical expression that Urbach energy can be calculated[47]:

$$\alpha = \alpha_0 \exp\left(\frac{h\upsilon - E_0}{E_U}\right) \qquad [6]$$

where E_0 and α_0 are characteristic parameters of the material and E_U is the Urbach energy which refers to the width of the exponential absorption edge. The Urbach energy (E_U) values were calculated from the variation of $\ln\alpha$ vs. photon energy[48] and given in Table III. Besides the thermal component to the structural disorder mechanism, there is an additional non-thermal component to the disorders (defects in crystal structures).[49] Urbach energy values of the films increase with Mn incorporation. The optical band gaps of the films change reversely with Urbach energy values. This result causes a redistribution of states, such as from band to tail and tail to tail transitions[50] and in turn, the optical gap decreases due to the broadening of the Urbach tail. It can be seen that Mn incorporation causes a significant increase in the Urbach energy, compared to ZnO films, as a result of increasing structural disorder. According to our knowledge, there is only one study which is published by Caglar et al.[51] investigating the Urbach energy and steepness parameters in MZO films.

Equation [6] can be rewritten as

$$\alpha = \alpha_0 \exp\left(\frac{\delta(h\upsilon - E_0)}{k_B T}\right). \qquad [7]$$

where δ is called steepness parameter, which characterizes the steepness of the straight line near the absorption edge due to the electron-phonon interaction or exciton-phonon interaction,[51] k_B is the Boltzmann constant and T is the temperature. If E_U is related to the slope of Eq. [7], the δ parameter is found as

$$\delta = k_B T / E_U \qquad [8]$$

The δ values were calculated using Eq. [8] and letting $T = 300$ K (27 °C), which are given in Table III. Figure 6 shows the Urbach Energy vs. steepness parameter for the undoped ZnO and MZO (0.25, 0.50, and 0.75 mol pct values Mn-doped) thin films. As clearly seen from Figure 6, the steepness parameters become smaller as the Urbach energy values increase with increasing content of Mn in MZO. 18.3 meV difference in Urbach energy is observed as the Mn doping concentration increases from 0 to 0.75 mol pct.

IV. CONCLUSIONS

Undoped ZnO and MZO thin films have been successfully grown by a sol-gel spin-coating technique. XRD patterns of the films have showed strong c-axis-oriented crystal structure with preferred (002) orientation. Any of secondary phases related to oxides or groups of Mn were not observed. Although the
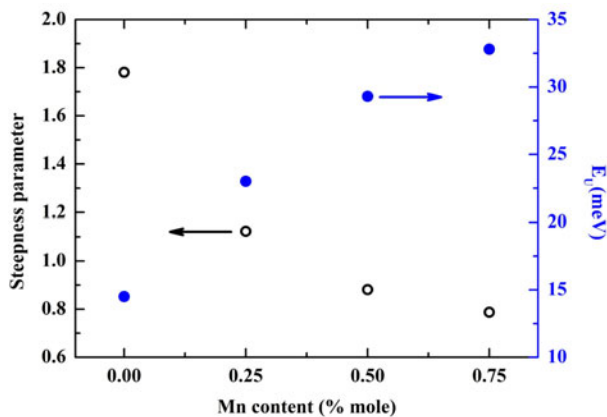
Fig. 6—Plot of Urbach energies and steepness parameters *vs.* different mole percent values of Mn.

dominant diffraction peak for the undoped ZnO and MZO thin films was (002), some other (100), (101), (102), (110), (103), (112), and (004) peaks with lesser intensities were also observed for the undoped ZnO. The lattice parameters were calculated, and it can be seen that the lattice parameters of MZO thin films are slightly lower than those of the undoped ZnO. Plane stress values were calculated, and the positive sign in front of these values indicated that the films had the tensile stress. From the AFM analyses, with increasing Mn mole percent, the grain growth orientation is perpendicular to the substrate surface, and smaller grain sizes which are compatible with the XRD patterns were observed. The optical transmission values, at the wavelength of 405 nm, were found to be 82 pct for the undoped ZnO and 80, 78, and 75 pct for the MZO with 0.25, 0.50 and 0.75 mol pct, respectively. The optical band gap values decreased from 3.287 to 3.270 eV, and the surface roughness values increased from 58.13 to 60.67 nm upon increasing the Mn content from 0.0 to 0.75 mol pct. Although the steepness parameters decreased, the Urbach energy values increased, and a 18.3 meV difference in Urbach energy was observed with increasing Mn content from 0.0 to 0.75 mol pct. From the results of this study, the undoped ZnO and MZO thin films are the perfect candidate materials in terms of optical and structural parameters for the preparation of superlattices, quantum wells, and other applications in the band gap engineering industry.

REFERENCES

1. A.U. Ubale and V.P. Deshpande: *J. Alloy. Compd.*, 2010, vol. 500, pp. 138–43.
2. Ü. Özgür, Y.I. Alivov, C. Liu, A. Teke, S. Doğan, M. Reshchikov, V. Avrutin, S.J. Cho, and H. Morkoç: *J. Appl. Phys.*, 2005, vol. 98, pp. 041301–404.
3. W. Gao and Z. Li: *Ceram. Int.*, 2004, vol. 30, pp. 1155–59.
4. A. Hongsingthong, I. Afdi Yuna, S. Miyajima, and M. Konagai: *Sol. Energy Mater. Sol. Cells*, 2011, vol. 95, pp. 171–74.
5. D. Kim, I. Yun, and H. Kim: *Curr. Appl. Phys.*, 2010, vol. 10, pp. 459–62.
6. W. Lin, R. Ma, J. Xue, and B. Kang: *Sol. Energy Mater. Sol. Cells*, 2007, vol. 91, pp. 1902–05.
7. H. Zhu, J. Hupkes, E. Bunte, A. Gerber, and S.M. Huang: *Thin Solid Films*, 2010, vol. 518, pp. 4997–5002.
8. S. Faÿ, J. Steinhauser, S. Nicolay, and C. Ballif: *Thin Solid Films*, 2010, vol. 518, pp. 2961–66.
9. O.D. Jayakumar, I.K. Gopalakrishnan, C. Sudakar, and S.K. Kulshreshtha: *J. Cryst. Growth*, 2006, vol. 294, pp. 432–36.
10. X. Zhou, Q. Xue, H. Chen, and C. Liu: *Physica E*, 2010, vol. 42, pp. 2021–25.
11. H.-J. Lim, D.Y. Lee, and Y.-J. Oh: *Sens. Actuators A*, 2006, vol. 125, pp. 405–10.
12. P.P. Sahay and R.K. Nath: *Sens. Actuators B*, 2008, vol. 134, pp. 654–59.
13. V. Khranovskyy, U. Grossner, O. Nilsen, V. Lazorenko, G.V. Lashkarev, B.G. Svensson, and R. Yakimova: *Thin Solid Films*, 2006, vol. 515, pp. 472–76.
14. V.R. Shinde, T.P. Gujar, C.D. Lokhande, R.S. Mane, and S.-H. Han: *Mater. Chem. Phys.*, 2006, vol. 96, pp. 326–30.
15. H.B. Ruan, L. Fang, D.C. Li, M. Saleem, G.P. Qin, and C.Y. Kong: *Thin Solid Films*, 2011, vol. 519, pp. 5078–81.
16. J. Elanchezhiyan, K.P. Bhuvana, N. Gopalakrishnan, and T. Balasubramanian: *Mater. Lett.*, 2008, vol. 62, pp. 3379–81.
17. P. Singh, A. Kaushal, and D. Kaur: *J. Alloy. Compd.*, 2009, vol. 471, pp. 11–15.
18. J. Heber: *Nature*, 2009, vol. 459, pp. 28–30.
19. D.C. Kim, B.H. Kong, S.O. Jun, H.K. Cho, D.J. Park, and J.Y. Lee: *Thin Solid Films*, 2008, vol. 516, pp. 5562–66.
20. L.P. Dai, H. Deng, J.J. Chen, and M. Wei: *Solid State Commun.*, 2007, vol. 143, pp. 378–81.
21. A. Barnabé, M. Lalanne, L. Presmanes, J.M. Soon, Ph. Tailhades, C. Dumas, J. Grisolia, A. Arbouet, V. Paillard, G. BenAssayag, M.A.F. vandenBoogaart, V. Savud, J. Brugge, and P. Normand: *Thin Solid Films*, 2009, vol. 518, pp. 1044–47.
22. Y. Feng, Y. Zhou, Y. Liu, G. Zhang, and X. Zhang: *J. Lumin.*, 2006, vols. 119–120, pp. 233–36.
23. X.Q. Zhang, I. Suemune, H. Kumano, Z.G. Yao, and S.H. Huang: *J. Lumin.*, 2007, vols. 122–123, pp. 828–30.
24. J.S. Kang, H.S. Kang, S.S. Pang, E.S. Shim, and S.Y. Lee: *Thin Solid Films*, 2003, vol. 443, pp. 5–8.
25. V. Narayanan and R.K. Thareja: *Opt. Commun.*, 2006, vol. 260, pp. 170–74.
26. Y. Wu, L. Zhang, G. Xie, J. Ni, and Y. Chen: *Solid State Commun.*, 2008, vol. 148, pp. 247–50.
27. D. Wang, J. Zhou, and G. Liu: *J. Alloy. Compd.*, 2009, vol. 487, pp. 545–49.
28. C.-Y. Tsay, H.-C. Cheng, Y.-T. Tung, W.-H. Tuan, and C.-K. Lin: *Thin Solid Films*, 2008, vol. 517, pp. 1032–36.
29. R. Khandelwal, A.P. Singh, A. Kapoor, S. Grigorescu, P. Miglietta, N.E. Stankova, and A. Perrone: *Opt. Laser Technol.*, 2008, vol. 40, pp. 247–51.
30. A. Chakraborty, T. Mondal, S.K. Bera, S.K. Sen, R. Ghosh, and G.K. Paul: *Mater. Chem. Phys.*, 2008, vol. 112, pp. 162–66.
31. K.J. Chen, F.Y. Hung, S.J. Chang, and S.J. Young: *J. Alloy. Compd.*, 2009, vol. 479, pp. 674–77.
32. Y. Liu, S. Yang, Y.L. Zhang, and D.H. Bao: *J. Magn. Magn. Mater.*, 2009, vol. 321, pp. 3406–10.
33. T. Dietl, H. Ohno, F. Matsukura, J. Cibert, and D. Ferrand: *Science*, 2000, vol. 287, pp. 1019–22.
34. E.F. Keskenler, S. Doğan, B. Diyarbakır, S. Duman, and B. Gürbulak: *J. Sol–Gel. Sci. Technol.*, 2011, vol. 60, pp. 66–70.
35. U.N. Maiti, P.K. Ghosh, S. Nandy, and K.K. Chattopadhyay: *Physica B*, 2007, vol. 387, pp. 103–08.
36. G. Srinivasan and J. Kumar: *J. Cryst. Growth*, 2008, vol. 310, pp. 1841–46.
37. D. Shuang, J.B. Wang, X.L. Zhong, and H.L. Yan: *Mater. Sci. Semicond. Proc.*, 2007, vol. 10, pp. 97–102.
38. A. Bowen, J. Li, J. Lewis, K. Sivaramakrishnan, T.L. Alford, and S. Iyer: *Thin Solid Films*, 2011, vol. 519, pp. 1809–16.
39. S. Maniv, W.D. Westwood, and E. Colombini: *J. Vac. Sci. Technol.*, 1982, vol. 20, pp. 162–70.
40. O. Takai, M. Futsuhara, G. Shimizu, C.P. Lungu, and J. Nozue: *Thin Solid Films*, 1998, vol. 318, pp. 117–19.
41. J. Bardeen and W. Shockley: *Phys. Rev.*, 1950, vol. 80, pp. 72–80.

42. R. Cebulla, R. Wendt, and K. Ellmer: *J. Appl. Phys.*, 1998, vol. 83, pp. 1087–95.
43. S.-Y. Chu, W. Water, and J.-T. Liaw: *J. Eur. Ceram. Soc.*, 2003, vol. 23, pp. 1593–98.
44. J.M. Khoshman and M.E. Kordesch: *Thin Solid Films*, 2007, vol. 515, pp. 7393–99.
45. M. Caglar, S. Ilican, Y. Caglar, and F. Yakuphanoglu: *Appl. Surf. Sci.*, 2009, vol. 255, pp. 4491–96.
46. S.K. Sinha, T. Rakshit, S.K. Ray, and I. Manna: *Appl. Surf. Sci.*, 2011, vol. 257, pp. 10551–56.
47. F. Urbach: *Phys. Rev.*, 1953, vol. 92, pp. 1324–25.
48. M.H. Mamat, M.Z. Sahdan, S. Amizam, H.A. Rafaie, Z. Khusaimi, and M. Rusop: *J. Ceram. Soc. Jpn.*, 2009, vol. 117, pp. 1263–67.
49. G.D. Cody, T. Tiedje, B. Abeles, B. Brooks, and Y. Goldstein: *Phys. Rev. Lett.*, 1981, vol. 47, pp. 1480–83.
50. S.K. O'Leary, S. Zukotynski, and J.M.J. Perz: *Non-Cryst. Solids*, 1997, vol. 210, pp. 249–53.
51. Y. Caglar, S. Ilican, M. Caglar, and F. Yakuphanoglu: *J. Sol–Gel. Sci. Technol.*, 2010, vol. 53, pp. 372–77.